

## Sub-diffraction imaging with compensating bilayers

**D Schurig and D R Smith**

Department of Electrical and Computer Engineering, Duke University,  
Box 90291, Durham, NC 27708, USA

E-mail: [dschurig@duke.edu](mailto:dschurig@duke.edu)

*New Journal of Physics* **7** (2005) 162

Received 19 April 2005

Published 8 August 2005

Online at <http://www.njp.org/>

doi:10.1088/1367-2630/7/1/162

**Abstract.** We derive a general expression for the material properties of a compensating bilayer, which is a pair of material layers which transfer the field distribution from one side of the bilayer to the other with resolution limited only by the deviation of the material properties from specified values. One of the layers can be free space, a special case of which is the perfect lens, but the layers need not have equal thickness. Compensating a thick layer of free space with a thin layer creates a focusing device with increased working distance, and employs an anisotropic material. It is also possible to achieve compensation of materials with property tensors that are neither positive nor negative definite. In this case, we refer to such media as indefinite, and we analyse, in detail, bilayers of these media which support coupling of internal propagating waves to incident waves of any transverse wave vector. In this case, we find that the enhanced spatial resolution provided by large transverse wave vectors is far less sensitive to loss than that of the perfect lens.

**Contents**

<b>1. Introduction</b>	<b>2</b>
<b>2. Dispersion</b>	<b>3</b>
<b>3. General bilayer solution</b>	<b>5</b>
<b>4. Compensating free space</b>	<b>7</b>
<b>5. Perfectly Matched Layer (PML)</b>	<b>8</b>
<b>6. Never cutoff bilayer</b>	<b>9</b>
<b>7. Lossy media: approximate analytical transfer function</b>	<b>12</b>
<b>8. Conclusion</b>	<b>13</b>
<b>Acknowledgments</b>	<b>14</b>
<b>References</b>	<b>14</b>

**1. Introduction**

Negative refractive index, first considered theoretically by Veselago [1], has been demonstrated in structured metamaterials and photonic band gap materials [2]–[5]. Many fundamental aspects of wave propagation are significantly modified in negative refractive index materials—a result of the intrinsic reversal of phase and group velocities associated with plane waves. Veselago, for example, showed that unusual geometrical optics could be expected from negative index materials, including convex lenses that would act as concave lenses, and vice versa. Veselago [1] also predicted that a planar slab of material having permittivity ( $\epsilon$ ) and permeability ( $\mu$ ) both equal to  $-1$  could produce an image on one side of the slab from a source placed on the opposite side.

The imaging properties of a planar slab of negative index material gained considerable attention when Pendry, after applying a Fourier optics analysis [6], concluded that the images produced could have significantly higher spatial resolution than that associated with the diffraction limit. Pendry expanded an object field in both homogeneous (propagating) and inhomogeneous (evanescent) plane waves, and calculated the transfer function (i.e., the field at the image plane divided by the field at the object plane) for each component. He then noted that, in addition to the focusing of the homogeneous components, the magnitude of the inhomogeneous components was restored; that is, the exponentially decaying field components, normally lost using conventional positive index optics, are converted to exponentially growing waves in the negative index material so as to be recovered at the image. In a hypothetical isotropic material having  $\epsilon = -1$  and  $\mu = -1$  with no losses, an exact reproduction of the source can in principle be obtained, and thus Pendry called this focusing slab a ‘perfect lens’.

Of course, limitations inherent to realizable materials reduce the achievable resolution of a negative index slab. Pendry noted, for example, that losses would introduce a natural limit to the resolution of the ‘perfect lens’. Other researchers have also noted the difficulties associated with obtaining enhanced resolution images using the ‘perfect lens’ configuration [7]–[10]. However, recent demonstrations have obtained resolution modestly better than the diffraction limit of traditional optics [11].

The ‘perfect lens’ proposed by Pendry can be viewed as a pair of slabs—or a bilayer, in which the negative index material exactly compensates for the propagation effects associated

with an equal length of vacuum. In this sense, the negative index material has the properties of ‘anti-vacuum’ [12], reversing the phase advance of homogeneous plane wave components and the exponential decay of inhomogeneous plane wave components. The composite bilayer has the property that the net transfer function for each plane wave component is unity. The perfect lens configuration can be generalized to layers of unequal thickness. The layer of free space being compensated may be either thicker or thinner than the material (lens) layer. In the former case, this allows for an increased working distance, which may be quite desirable in some applications. The unequal layer compensation of free space requires anisotropic media.

Bilayer compensation can also be accomplished using anisotropic materials having indefinite permittivity and permeability tensors; that is, not all elements of the permittivity or permeability tensors have the same sign [13]. A configuration that will be discussed here at length is a compensated bilayer that employs a particular class of media, which we refer to as ‘never cutoff’ [14]. An unusual property of this medium is that it is characterized by a hyperbolic dispersion relation that supports propagating waves for all transverse wave vectors. A similar type of wave propagation behaviour can be observed in the plasma cones that occur in anisotropic plasmas [15, 16]. Even plane waves that would be evanescent in free space, when incident on this medium, are converted to propagating waves. There are two sub-classes of never cutoff indefinite materials, one positive refracting and the other negative refracting, that together can satisfy the requirements for a compensated bilayer. Because all plane wave components from the source fields in a never cutoff material are bounded, the compensated bilayers presented here can produce enhanced resolution images that exhibit a decreased sensitivity to losses and to deviations in material parameters relative to the ‘perfect lens’ configuration. These configurations, however, provide no free space working distance.

## 2. Dispersion

The electromagnetic properties of continuous anisotropic materials are generally described by their permittivity and permeability tensors  $\boldsymbol{\epsilon}$  and  $\boldsymbol{\mu}$ . To simplify the analysis that follows, we assume a material whose  $\boldsymbol{\epsilon}$  and  $\boldsymbol{\mu}$  tensors are simultaneously diagonalizable in an orthogonal basis having the diagonal form,

$$\boldsymbol{\epsilon} = \begin{pmatrix} \epsilon_x & 0 & 0 \\ 0 & \epsilon_y & 0 \\ 0 & 0 & \epsilon_z \end{pmatrix} \quad \text{and} \quad \boldsymbol{\mu} = \begin{pmatrix} \mu_x & 0 & 0 \\ 0 & \mu_y & 0 \\ 0 & 0 & \mu_z \end{pmatrix}. \quad (1)$$

We restrict the polarization, such that the electric field is directed along the  $y$ -axis. Maxwell’s equations thus reduce to the following scalar wave equation

$$\left( \frac{1}{\mu_z} \frac{\partial^2}{\partial x^2} + \frac{1}{\mu_x} \frac{\partial^2}{\partial z^2} \right) E_y = \epsilon_y \frac{\partial^2}{\partial t^2} E_y. \quad (2)$$

Assuming plane wave solutions of the form

$$\mathbf{E} = \hat{\mathbf{y}} e^{i(k_x x + k_z z - \omega t)}, \quad (3)$$

we find the following dispersion relation:

$$k_z^2 = \epsilon_y \mu_x \frac{\omega^2}{c^2} - \frac{\mu_x}{\mu_z} k_x^2. \quad (4)$$

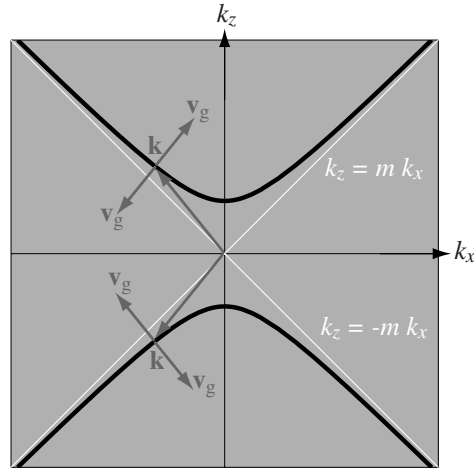


**Figure 1.** Hyperbolic dispersion found in never cutoff media (black). The asymptotic behaviour is also shown (white). Two wave vectors are shown that have the same transverse component,  $k_x$ . Both possible group velocity directions are shown for each wave vector. The normal ( $z$ ) components of  $\mathbf{k}$  and  $\mathbf{v}_g$  can be either of the same sign or opposite sign.

In the subsequent analysis, the layered media will have interfaces normal to the  $z$ -axis. The domain of the solution will be unbounded in the  $x$  and  $y$  directions and we will consider only real  $k_x$ .

The sign of  $k_z^2$  determines the nature of the plane wave solutions. Positive  $k_z^2$  corresponds to real valued  $k_z$  and propagating solutions. Negative  $k_z^2$  corresponds to imaginary  $k_z$  and exponentially growing and decaying (evanescent) solutions. A concise summary of the wave propagation properties of the media is given by the shape of the iso-frequency surface in  $k$ -space, given by equation (4) [13]. In our analysis, we will consider materials that have spherical, elliptical and hyperbolic surfaces. The least familiar are the hyperbolic media. One type of hyperbolic media of particular interest satisfies

$$\varepsilon_y \mu_x > 0 \quad \text{and} \quad \frac{\mu_x}{\mu_z} < 0. \quad (5)$$

This condition requires material property tensors whose principal values are not all of the same sign. The hyperbolic surfaces have asymptotes with slope,  $m$ , defined at large  $k_x$  by

$$m \equiv \left| \frac{\partial k_z}{\partial k_x} \right| = \left| \frac{k_z}{k_x} \right| = \sqrt{\left| \frac{\mu_x}{\mu_z} \right|}. \quad (6)$$

We refer to such materials as never cutoff.

As will be seen below, the slope,  $m$ , is directly observable in spatial field intensity patterns, and is a signature of the hyperbolic dispersion. The iso-frequency curves corresponding to the two branches of the dispersion relation equation (4) are shown in figure 1, where it can be noted that for all values of  $k_x$  there are real values of  $k_z$ . Since this curve is a constant frequency contour,  $\omega(\mathbf{k}) = \text{constant}$ , the group velocity,  $\mathbf{v}_g \equiv \nabla_{\mathbf{k}} \omega(\mathbf{k})$ , must be normal to the curve. From the figure, one can see that at large  $k_x$ ,  $\mathbf{v}_g$  will also be normal to  $\mathbf{k}$ . There are two types of never

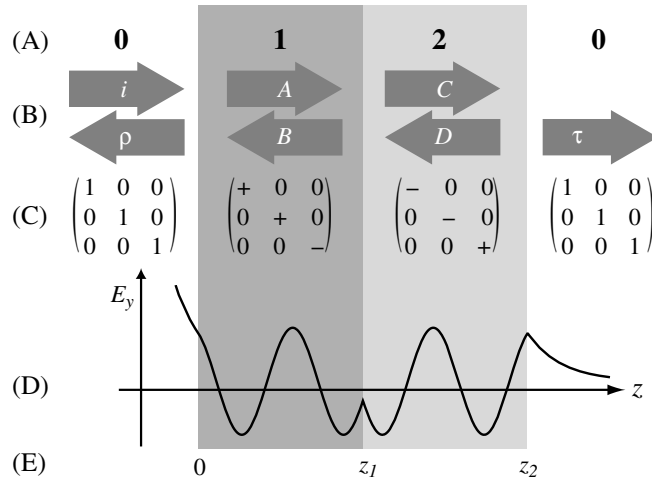


**Figure 2.** From top to bottom: (A) the indices used to refer to material properties, (B) the conventions for the coefficients of each component of the general solution, (C) the sign structure of the material property tensors for a never cutoff bilayer, (D) typical  $z$ -dependence of the electric field for an evanescent incident plane wave, (E)  $z$ -coordinate of the interfaces.

cutoff material that correspond to the two possible directions of the group velocity. Particularly simple tensor forms for these two types of never cutoff media are given in equation (32).

### 3. General bilayer solution

We first solve the general problem of an S-polarized wave incident on an anisotropic bilayer with unequal layer thickness. The property tensors are assumed simultaneously diagonalizable in an orthogonal basis containing the layer normal, as in equation (1). The general solution for the electric field with unknown coefficients is given by,

$$E_y = e^{i(k_x x - \omega t)} \begin{cases} e^{ik_z z} + \rho e^{-ik_z z} & z < 0, \\ Ae^{ip_z z} + Be^{-ip_z z} & 0 < z < z_1, \\ Ce^{iq_z z} + De^{-iq_z z} & z_1 < z < z_2, \\ \tau e^{ik_z z} & z_2 < z. \end{cases} \quad (7)$$

The  $z$ -components of the wave vectors are found from the dispersion relation, equation (4),

$$k_z = \pm \sqrt{k_0^2 - k_x^2}, \quad (8a)$$

$$p_z = \pm \sqrt{\varepsilon_{1y} \mu_{1x} k_0^2 - \frac{\mu_{1x}}{\mu_{1z}} k_x^2}, \quad (8b)$$

$$q_z = \pm \sqrt{\varepsilon_{2y} \mu_{2x} k_0^2 - \frac{\mu_{2x}}{\mu_{2z}} k_x^2}, \quad (8c)$$

where  $k_0 = \omega/c$  and the material parameters are relative to free space. The conventions for the material property subscripts and solution coefficients are shown in figure 2. The general solution includes exponentials with both signs of  $p_z$  and  $q_z$ , so a choice of sign for these square roots is unnecessary. We choose the branch of the square root for  $k_z$ , such that  $k_z$  is either real and positive or imaginary and positive, ensuring that the incident wave propagates toward the bilayer or decays in the direction toward the bilayer (away from the source). The transverse component ( $y$ ) of the electric field is conserved across each of the three interfaces, at  $z = 0$ ,  $z = z_1$  and  $z = z_2$ , yielding three equations. The transverse magnetic component, given by

$$H_x = -\frac{1}{\omega} e^{i(k_x x - \omega t)} \begin{cases} k_z (e^{ik_z z} - \rho e^{-ik_z z}) & z < 0, \\ \frac{p_z}{\mu_{1x}} (Ae^{ip_z z} - Be^{-ip_z z}) & 0 < z < z_1, \\ \frac{q_z}{\mu_{2x}} (Ce^{iq_z z} - De^{-iq_z z}) & z_1 < z < z_2, \\ k_z \tau e^{ik_z z} & z_2 < z. \end{cases} \quad (9)$$

is also conserved at the three interfaces and yields three more equations. The six boundary matching equations are solved for the six unknown coefficients:  $\rho$ ,  $A$ ,  $B$ ,  $C$ ,  $D$ ,  $\tau$ . The transfer function from the front surface to the back surface of the bilayer is given by the ratio of the transmitted electric field to the incident electric field

$$T = \frac{E_y(k_x, z = z_2)}{E_{yi}(k_x, z = 0)} = \tau e^{ik_z z_2}. \quad (10)$$

Inserting the value of  $\tau$  from the solution of the system of six equations yields

$$T = 8 \left[ \frac{e^{i(\phi+\psi)}(1-Z_0)(1+Z_1)(1-Z_2) + e^{i(\phi-\psi)}(1-Z_0)(1-Z_1)(1+Z_2) + e^{-i(\phi-\psi)}(1+Z_0)(1-Z_1)(1-Z_2) + e^{-i(\phi+\psi)}(1+Z_0)(1+Z_1)(1+Z_2)}{e^{i(\phi+\psi)}(1-Z_0)(1+Z_1)(1-Z_2) + e^{i(\phi-\psi)}(1-Z_0)(1-Z_1)(1+Z_2) + e^{-i(\phi-\psi)}(1+Z_0)(1-Z_1)(1-Z_2) + e^{-i(\phi+\psi)}(1+Z_0)(1+Z_1)(1+Z_2)} \right]^{-1}, \quad (11)$$

where the effective relative impedances are given by

$$Z_0 \equiv \frac{p_z}{\mu_{1x} k_z}, \quad Z_b \equiv \frac{\mu_{1x} q_z}{\mu_{2x} p_z}, \quad Z_2 \equiv \frac{\mu_{2x} k_z}{q_z}, \quad (12)$$

and the individual layer phase advance angles are defined as

$$\phi \equiv p_z z_1 \quad \text{and} \quad \psi \equiv q_z (z_2 - z_1). \quad (13)$$

To obtain a unit transfer function,  $T = 1$ , it is sufficient that

$$\phi \pm \psi = 0 \quad \text{and} \quad 1 \mp Z_1 = 0. \quad (14)$$

These two conditions are equivalent to layer compensation as discussed above, and the additional requirement of an impedance match between the layers. Note that the individual layers need not be matched to the surrounding media. The sign choice is determined by the sign choice in equation (8a) and (8b), i.e., it is arbitrary. We will use the upper sign in what follows, but either choice will lead to the same result.

From equations (13) and (14), we have

$$p_z = -r q_z, \quad (15)$$

where the thickness ratio  $r$  is defined as

$$r \equiv \frac{z_2 - z_1}{z_1}. \quad (16)$$

Combining equation (15) with equations (12) and (14), we find the first material requirement,

$$\mu_{2x} = -\frac{1}{r}\mu_{1x}. \quad (17)$$

Squaring equation (15) and using equation (8), we obtain

$$\varepsilon_{1y}\mu_{1x}k_0^2 - \frac{\mu_{1x}}{\mu_{1z}}k_x^2 = r^2\varepsilon_{2y}\mu_{2x}k_0^2 - r^2\frac{\mu_{2x}}{\mu_{2z}}k_x^2. \quad (18)$$

For this to be valid for all  $k_x$ , we must have

$$\varepsilon_{1y}\mu_{1x} = r^2\varepsilon_{2y}\mu_{2x} \quad \text{and} \quad \frac{\mu_{1x}}{\mu_{1z}} = r^2\frac{\mu_{2x}}{\mu_{2z}}. \quad (19)$$

Combining this with the first material requirement, equation (17), we obtain two more material requirements, so that the total material requirements for an S-polarization compensated bilayer,

$$\varepsilon_{2y} = -\frac{1}{r}\varepsilon_{1y}, \quad \mu_{2x} = -\frac{1}{r}\mu_{1x} \quad \text{and} \quad \mu_{2z} = -r\mu_{1z}. \quad (20)$$

We can find the requirements for a P-polarization compensated bilayer by swapping  $\mu$  and  $\varepsilon$ ,

$$\mu_{2y} = -\frac{1}{r}\mu_{1y}, \quad \varepsilon_{2x} = -\frac{1}{r}\varepsilon_{1x} \quad \text{and} \quad \varepsilon_{2z} = -r\varepsilon_{1z}. \quad (21)$$

Thus, for a polarization independent compensating bilayer the requirement is

$$\boldsymbol{\varepsilon}_2 = \boldsymbol{\psi}\boldsymbol{\varepsilon}_1 \quad \text{and} \quad \boldsymbol{\mu}_2 = \boldsymbol{\psi}\boldsymbol{\mu}_1, \quad (22)$$

where  $\boldsymbol{\psi}$ , which we will call the compensation matrix, is given by [17]

$$\boldsymbol{\psi} = \begin{pmatrix} -\frac{1}{r} & 0 & 0 \\ 0 & -\frac{1}{r} & 0 \\ 0 & 0 & -r \end{pmatrix}. \quad (23)$$

Recall that, we have assumed that  $\boldsymbol{\varepsilon}$  and  $\boldsymbol{\mu}$  are diagonal matrices and that the layers are oriented normal to the  $z$ -axis, thus equation (22) is not a tensor equation and we cannot apply it to media represented by non-diagonal matrices, such as non-orthorhombic media or even orthorhombic media with layer surfaces other than those along the symmetry axes.

#### 4. Compensating free space

The most well known example of a compensating bilayer is the perfect lens. In the perfect lens, a layer of media compensates a layer of free space of equal thickness. For layers of equal thickness,

$$\boldsymbol{\psi} = -\mathbf{I}, \quad (24)$$

where  $\mathbf{I}$  is the identity matrix. The free space layer being compensated has isotropic properties,

$$\varepsilon_1 = \mu_1 = 1, \quad (25)$$

which yields immediately,

$$\varepsilon_2 = \mu_2 = -1. \quad (26)$$

We can relax the condition of equal layer thickness in a generalization of the perfect lens. This may be desirable, if one wishes to have a free space working distance greater than the thickness of the lens. The price for this greater working distance is material properties less than  $-1$ , which may be more difficult to achieve in practice. In this case, the compensating layer has material properties equal to the compensation matrix, equation (23),

$$\varepsilon_2 = \mu_2 = \psi. \quad (27)$$

This results in the elliptical dispersion [18],

$$k_x^2 + r^2 k_z^2 = \frac{\omega^2}{c^2}. \quad (28)$$

We note that the perfect lens, with  $r = 1$ , has circular dispersion, like free space. In practice, relative material properties on the order of  $-3$  have been achieved, which would make a three to one working distance to lens thickness possible.

## 5. Perfectly Matched Layer (PML)

The compensation matrix, equation (23), will look familiar to those who work with finite difference or finite element simulations. It is often useful to simulate semi-infinite media with these techniques. This is done by creating a PML, i.e., a layer with a reflection coefficient of zero for all angles of incidence. The requirements for a PML are less strict than a compensating bilayer. A PML only requires zero reflection between two semi-infinite regions; this is equivalent to the impedance condition,

$$Z_1 = 1, \quad (29)$$

but the phase compensation condition,

$$\phi + \psi = 0, \quad (30)$$

is not necessary. This is why the PML properties to match to free space, for example,

$$\varepsilon = \mu = \begin{pmatrix} \alpha + i\beta & 0 & 0 \\ 0 & \alpha + i\beta & 0 \\ 0 & 0 & \frac{1}{\alpha + i\beta} \end{pmatrix}, \quad (31)$$

are always used with positive real parts, though negative real parts would also work. The imaginary part,  $\beta$ , is made sufficiently large, to attenuate incident waves to negligible amplitude on a round trip through the layer (the layer must of course be of finite thickness). Note that since a complex value and its reciprocal both appear, this material is necessarily active, and cannot be implemented with passive materials; this fact is irrelevant for numerical simulations, but precludes all angle, broadband absorption by real, passive materials, which would of course be desirable.

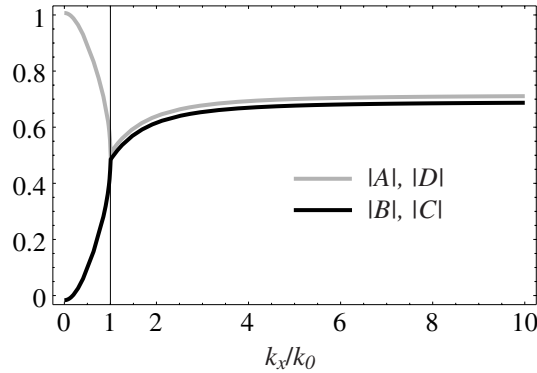


**Figure 3.** The magnitude of coefficients of the internal field components. For values of  $k_x > k_0$  (i.e. incident plane wave is evanescent), the forward and backward components have equal magnitude. The magnitude approaches  $1/\sqrt{2}$  when  $k_x \gg k_0$ .

## 6. Never cutoff bilayer

To illustrate the focusing properties of a never cutoff compensated bilayer, we consider a medium with material parameters given by

$$\boldsymbol{\varepsilon}_1 = \boldsymbol{\mu}_1 = \begin{pmatrix} 1 & 0 & 0 \\ 0 & 1 & 0 \\ 0 & 0 & -1 \end{pmatrix} \quad \text{and} \quad \boldsymbol{\varepsilon}_2 = \boldsymbol{\mu}_2 = \begin{pmatrix} -1 & 0 & 0 \\ 0 & -1 & 0 \\ 0 & 0 & 1 \end{pmatrix}. \quad (32)$$

In this case (as with all others discussed in this paper), we will choose the  $\boldsymbol{\varepsilon}$  and  $\boldsymbol{\mu}$  tensors equal to each other, thus ensuring that the focusing properties are independent of polarization. We also choose these tensors to be  $x$ - $y$  isotropic, so that the focusing properties are independent of the  $x$ - $y$  orientation of the layers. For convenience, we further choose unit magnitude for all tensor components.

To transfer an image across a bilayer made from the indefinite materials defined by equation (32), the layer thicknesses must be equal,  $z_1 = z_2 - z_1 \equiv d$ . Using these values in equations (8) and (11)–(13), we find the transfer function is unity for all incident plane waves; that is  $T = 1$  for all  $k_x$  values. The magnitude is preserved and the phase advance across the bilayer is zero. We will consider deviation from this ideal condition below.

The compensated bilayer achieves image resolution beyond the diffraction limit by converting the evanescent components of the source field distribution into propagating modes, and then back to evanescent fields on the opposite side of the bilayer. The mechanism of enhanced resolution of the bilayer is thus due to the excitation of a standing wave mode in the material, as opposed to the excitation of coupled surface plasmons in the ‘perfect lens’. The principle of operation of the bilayer can be understood by considering the manner, in which energy is transported from one side to the other.

In steady state, evanescent incident waves ( $k_x/k_0 > 1$ ) carry no net energy across the bilayer, but on entering the bilayer they are converted to propagating waves. Since propagating waves do carry energy, coefficients for the forward and backward waves in each layer must be equal; the standing wave ratio must be unity. From a plot of the internal field coefficients, shown in figure 3, we see that this is indeed the case:  $|A| = |B|$  and  $|D| = |C|$  for  $k_x/k_0 > 1$ .

In contrast, propagating incident waves do transfer energy across the bilayer. As shown in figure 3, for propagating incident waves ( $k_x/k_0 < 1$ ), the forward coefficient,  $A$ , is larger in magnitude than the backward coefficient,  $B$ . These roles are reversed in the second layer,  $|D| > |C|$ . The second layer is a negative refracting material, in which the  $z$ -component of the wave vector and group velocity have opposite signs. The wave associated with coefficient  $D$  has a negative  $z$ -component of the wave vector but a positive  $z$ -component of the group velocity. This wave must have larger magnitude than the one associated with  $C$ , to obtain a net power flow across the layer in the positive direction as conservation of energy requires. The net  $z$ -component of the group velocity must be positive in both layers to conserve energy across the interfaces.

The electric field takes a particularly simple form in the limit  $k_x \gg k_0$ .

$$E_y = e^{i(k_x x - \omega t)} \begin{cases} e^{-k_x z} & z < 0, \\ \sqrt{2} \cos[k_x z + \pi/4] & 0 < z < d, \\ \sqrt{2} \cos[k_x(2d - z) + \pi/4] & d < z < 2d, \\ e^{-k_x(z-2d)} & 2d < z, \end{cases} \quad (33)$$

where we see that the internal field is indeed a standing wave, and is symmetric about the centre of the bilayer. This field pattern is shown in figure 2.

We can obtain more general focusing configurations by relaxing the above symmetry. In the previous discussion, the property tensor elements all had unit magnitude leading to a dispersion slope of one, as seen from equation (6). Introducing a different slope,  $m$ , as follows

$$\varepsilon_1 = \mu_1 = \begin{pmatrix} m_1 & 0 & 0 \\ 0 & m_1 & 0 \\ 0 & 0 & -1/m_1 \end{pmatrix}, \quad (34a)$$

$$\varepsilon_2 = \mu_2 = \begin{pmatrix} -m_2 & 0 & 0 \\ 0 & -m_2 & 0 \\ 0 & 0 & 1/m_2 \end{pmatrix} \quad (34b)$$

and allowing the slope to differ in each layer, we can still maintain a unit transfer function,  $T = 1$ , if we adjust the thickness of the layers appropriately, such that

$$\frac{z_2 - z_1}{z_1} = \frac{m_1}{m_2}. \quad (35)$$

We have still maintained polarization independence and  $x$ - $y$  isotropy.

To simulate the focusing properties of the bilayer, we construct a localized source field on the front surface of the bilayer using a Fourier series.

$$E_{yi}(x, z = 0) = \sum_{k_x} a_{k_x} e^{ik_x x}. \quad (36)$$

Figure 4 shows an ideal source profile similar to a double slit screen back illuminated with a normally incident plane wave. This figure also shows the source profile of an approximating Fourier series with a modest number of components. The number of components is restricted to shorten computation time, but a sufficient number are used to adequately demonstrate sub-diffraction limit focusing. In any case, a natural cutoff of the higher Fourier components would be obtained if loss were introduced, as will be discussed below.

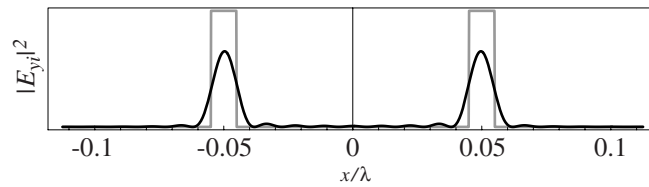


**Figure 4.** Field profile of an ideal source (grey) and an approximating Fourier series expansion (black) along the  $x$  direction.  $\lambda = 2\pi/k_0$ , is the free space wavelength. The components used in the expansion are:  $k_x = -N \cdot dk_x \dots 0 \dots N \cdot dk_x$ , where  $N = 20$  and  $dk_x/k_0 = 2.22$ .

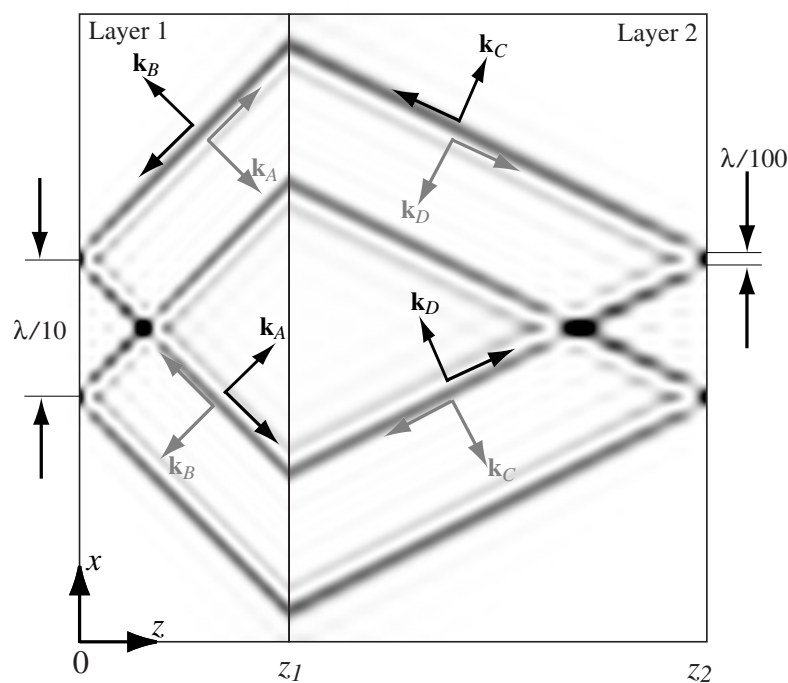


**Figure 5.** Internal electric field intensity plot for a localized two slit source. The four pairs of vectors in each layer indicate the only four orientations of internal plane waves. Plane waves from positive  $k_x$  components of the source are indicated in black and negative in grey. The wave vectors are labelled with the solution component to which they correspond.  $\mathbf{k}_A$  and  $\mathbf{k}_C$  have positive  $z$ -components and  $\mathbf{k}_B$  and  $\mathbf{k}_D$  have negative  $z$ -components. The unmarked vector in each pair indicates the direction of the group velocity for that plane wave direction.  $m_1 = 1$  and  $m_2 = 1/2$ .

The approximating Fourier series is used to demonstrate the internal field structure of the bilayer (figure 5). In this figure, we see that the plane wave components interfere to form a field intensity pattern that is localized in four beams, two for each slit. This pattern is a two-dimensional version of resonance cone formation [15]. The beams diverge in the first layer and converge in the second layer to reproduce the incident field pattern on the far side. The plane waves that constructively interfere to form each beam have phase fronts parallel to the beam

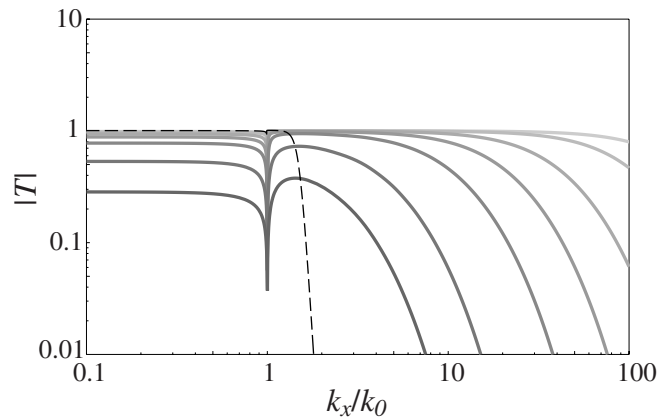


**Figure 6.** The transfer function from the front surface to the back surface of the bilayer.  $z_1 = z_2 - z_1 = \lambda$ ,  $m = 1/3$  and  $\varepsilon'' = \mu'' = 0.001, 0.002, 0.005, 0.01, 0.02, 0.05, 0.1$ , from light to dark. ( $\lambda = 2\pi/k_0$  is the free space wavelength.) For comparison, a ‘perfect’ lens is shown dashed. The ‘perfect’ lens has thickness,  $\lambda$ , and  $\varepsilon = \mu = -1 + 0.001i$ .

(i.e., the wave vector is perpendicular to the beam). The narrow slits yield a source dominated by large  $k_x$  components. These components lie well out on the asymptotes of the hyperbolic dispersion, so all of the wave vectors point in just four directions, as indicated in the plot. These directions correspond to the positive and negative  $k_x$  components in the source expansion and the forward and backward components of the solution ( $A, B$  or  $C, D$ ). Balmain *et al* has observed these field patterns in a two-dimensional, transmission line implementation of a never cutoff compensating bilayer [16].

## 7. Lossy media: approximate analytical transfer function

Lossy media is characterized by an imaginary component of the property tensors. We will use a single parameter for the imaginary component of all the principle elements of both  $\varepsilon$  and  $\mu$ .

$$\varepsilon_1 = \mu_1 = \begin{pmatrix} m + i\gamma & 0 & 0 \\ 0 & m + i\gamma & 0 \\ 0 & 0 & -1/m + i\gamma \end{pmatrix}, \quad (37a)$$

$$\varepsilon_2 = \mu_2 = \begin{pmatrix} -m + i\gamma & 0 & 0 \\ 0 & -m + i\gamma & 0 \\ 0 & 0 & 1/m + i\gamma \end{pmatrix}. \quad (37b)$$

For this analysis, we will use layers of equal slope and thickness,  $z_1 = z_2 - z_1 = d$ . Figure 6 shows the effect of loss on the transfer function. Increasing loss limits the  $k_x$  bandwidth. We can obtain a simple analytical approximation for the transfer function to see directly the trade-offs between bandwidth, slope, thickness and loss. We will assume that the loss parameter is small compared to the real part of the principal components of the material property tensors,

$\gamma \ll 1/m$ ,  $m$ , and further assume that  $k_x \gg k_0$ , limiting the range of validity of our approximate transfer function to large  $k_x$ . In spite of these assumptions, we find that the approximate transfer function agrees with the exact result over all values of  $k_x$ . In any case, it is of interest to find the  $k_x$  value that indicates the upper limit of the pass band, and this will typically occur at large  $k_x$ . Working to zeroth order, we obtain from equations (8a)–(8c)

$$k_z \approx ik_x, \quad (38a)$$

$$p_z \approx q_z \approx mk_x \quad (38b)$$

so that the effective impedances take the form

$$Z_0 \approx Z_2 \approx -i, \quad (39a)$$

$$Z_1 \approx -1. \quad (39b)$$

With these approximations the transfer function, equation (11), reduces to

$$T \approx \sec(\phi - \psi). \quad (40)$$

Expanding  $\phi$  and  $\psi$  to first-order, we obtain

$$T \approx \operatorname{sech}[k_x d(1 + m^2)\gamma]. \quad (41)$$

This approximate transfer function is in excellent agreement with the full expression, equation (11), in the appropriate limits. In particular, it accurately recovers the behaviour at large  $k_x$  values, where the transfer function rolls off. The dependence of bandwidth,  $\Delta k_x$ , on thickness,  $d$ , loss,  $\gamma$ , and slope,  $m$ , is given by

$$\Delta k_x d(1 + m^2)\gamma \sim 1. \quad (42)$$

Not surprisingly, larger bandwidth is obtained with thinner layers and smaller loss. Less intuitive is the role of the slope,  $m$ ; smaller slope gives larger bandwidth. In figure 5, we observe that a smaller slope corresponds to beams that lie on a more direct path through the layer. For fixed thickness,  $d$ , this means a shorter path. One might suggest that  $m = 0$ , with beams going straight through the layer, would be the most desirable. However, our analysis is only valid for  $m \gg \gamma$ . In addition, since  $1/m$  also appears as a principal component in the property tensors, there is a practical limit to how small  $m$  can be. Arbitrarily large  $\epsilon$  and  $\mu$  components are not realizable.

## 8. Conclusion

An important application of negative refractive materials is the compensation of the propagation effects associated with positive refractive materials. This type of compensation is available not only in isotropic materials, but also in anisotropic materials. However, because of the unusual dispersion characteristics associated with anisotropic indefinite media, structures composed of positive and negative refracting indefinite materials can result in bilayers with remarkable properties. The focusing bilayers presented here, which make use of never cutoff indefinite materials characterized by hyperbolic dispersion curves, represent an interesting and perhaps technologically useful example of propagation compensation.

In the focusing bilayer, an image is transmitted from one side of the bilayer to the other, including the inhomogeneous terms that would normally be excluded using positive index optical elements. The resulting image can thus display spatial resolution beyond that associated with the diffraction limit. In this sense, the compensated bilayer is quite similar to the ‘perfect lens’ proposed by Pendry [6]. However, a single layer of anisotropic material with negative refractive index cannot be used to compensate the propagation in free space, which is inherently isotropic. A negative refracting indefinite material can only compensate a positive refracting indefinite material with similar properties. So, unlike the ‘perfect lens’, a field distribution on one side of a bilayer is transferred to the other side, with no ‘working distance’ as is available with the ‘perfect lens’.

Yet, as we have shown, there are advantages to the imaging that can be obtained using indefinite media. Losses, which introduce a severe limitation to the ‘perfect lens’, are much less of a limitation to the sub-diffraction imaging in the bilayer. Here, the ultimate spatial resolution, given roughly by the bandwidth,  $\Delta k_x$ , is inversely proportional to the loss parameter, rather than exponentially related as with the ‘perfect lens’,  $\gamma \sim e^{-\Delta k_x d}$ . We note that Ramakrishnan and Pendry have considered the effect of sectioning a material with negative permittivity (positive permeability) into numerous thin slices [19]; they have found this configuration has a dependence on losses similar to equation (42) for the resolution. This composite structure is also highly anisotropic, and also sacrifices the working distance available with the original ‘perfect lens’ geometry.

The bilayers described here, can be formed from the same types of composite materials that were used in the experiments on negative refraction [2, 3]. In those experiments, a material with magnetic response to incident electromagnetic waves was formed using conducting split ring resonators, and combined with a conducting wire medium that provided an electric response. Over a band of microwave frequencies, both the effective permittivity and the effective permeability were found to be negative and nearly isotropic. An artificial medium utilizing the same types of scattering elements, but arranged so as to create an anisotropic response, would be appropriate to implement indefinite media.

Finally, we note that material properties can be equivalently understood in transmission line models using lumped circuit elements. Negative refractive media have been fabricated using series capacitance to introduce a negative permeability, and shunt inductance to introduce a negative permittivity, and have been used in planar circuits to demonstrate both focusing [20], and even the type of sub-diffraction focusing described here [16]. The fruitful interplay between material physics and electrical engineering will speed the implementation of indefinite materials and focusing bilayers, and open the door to practical applications.

## Acknowledgments

This work was supported by the DCI post-doctoral research fellowship programme, and by DARPA through grants from ONR (contract no. N00014-00-1-0632).

## References

- [1] Veselago V G 1968 *Sov. Phys.—Usp.* **10** 509
- [2] Smith D R, Padilla W, Vier D C, Nemat-Nasser S C and Schultz S 2000 *Phys. Rev. Lett.* **84** 4184

- [3] Shelby R A, Smith D R and Schultz S 2001 *Science* **292** 77
- [4] Notomi M 2000 *Phys. Rev. B* **62** 10696–705
- [5] Luo C, Johnson S G, Joannopoulos J D and Pendry J B 2002 *Phys. Rev. B* **65** 201104
- [6] Pendry J B 2000 *Phys. Rev. Lett.* **85** 3966–9
- [7] Shen J T and Platzman P M 2002 *Appl. Phys. Lett.* **80** 3286–8
- [8] Haldane F D M 2002 *Preprint* cond-mat/0206420
- [9] Ziolkowski R W and Heyman E 2001 *Phys. Rev. E* **6405** 056625
- [10] Smith D R, Schurig D, Rosenbluth M, Schultz S, Ramakrishnan S A and Pendry J B 2003 *Appl. Phys. Lett.* **82** 1506
- [11] Grbic A and Eleftheriades G V 2004 *Phys. Rev. Lett.* **92** 117403
- [12] Lakhtakia A 2002 *Int. J. Infrared Millim. Waves* **23** 339–43
- [13] Lindell I V, Tretyakov S A, Nikoskinen K I and Ilvonen S 2001 *Microwave Opt. Tech. Lett.* **31** 129
- [14] Smith D R and Schurig D 2003 *Phys. Rev. Lett.* **90** 077405
- [15] Fisher R K and Gould R W 1969 *Phys. Rev. Lett.* **22** 1093–5
- [16] Balmain K G, Luttgen A A E and Kremer P C 2002 *IEEE Antennas Wireless Propag. Lett.* **1** 146–9
- [17] Lakhtakia A and Sherwin J A 2003 *Int. J. Infrared Millim. Waves* **24** 19–23
- [18] Lu W and Sridhar S 2005 *Preprint* cond-mat/0501715
- [19] Ramakrishna S A, Pendry J B, Wiltshire M C K and Stewart W J 2003 *J. Mod. Opt.* **50** 1419–30
- [20] Iyer A K and Eleftheriades G V 2002 *2002 IEEE MTT-S International Microwave Symposium Digest* vol 2 (Piscataway, NJ: IEEE) pp 1067